Heliyon 10 (2024) e36160

Contents lists available at ScienceDirect

Heliyon

journal homepage: www.cell.com/heliyon

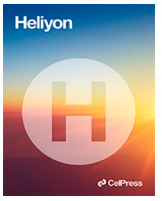

Research article

A novel approach for the modification of eggshell powder and its application for lead and methylene blue removal

Maherab Hossain [a], Raihan Islam [a], Mohammad Nurur Rahman [b], Md Ibna Sabit Khan [a], Firoz Ahmed [c], Md. Al-Amin [c], M. Ahasanur Rabbi [c,*]

[a] Department of Chemical & Food Process Engineering, Rajshahi University of Engineering &Technology, Rajshahi, 6204, Bangladesh
[b] Department of Chemical Engineering, Rajshahi University of Engineering & Technology, Rajshahi, 6204, Bangladesh
[c] BCSIR Rajshahi Laboratories, Bangladesh Council of Scientific and Industrial Research (BCSIR), Rajshahi, 6206, Bangladesh

ARTICLE INFO

Keywords:
Adsorbent
Magnetic composite
Chemical activation
Thermal activation
Active adsorption site
Surface saturation

ABSTRACT

Water pollution is one of the major concerns due to rapid industrialization and urbanization. Wastewater treatment has been an area of great interest for the researchers and among many technologies developed for water treatment, adsorption is the most preferred due to its efficiency and ability of been economical method. In this research, eggshell powder (ESP) is converted into modified eggshell powder (MESP) through chemical and thermal treatment (at 550 °C for 2 h) to use it as an adsorbent to remediate Pb^{2+} and Methylene blue (MB) from water, then it is transferred into modified eggshell powder magnetic composite (MESPMC) with iron coating to resolve the separation challenges and to boost the MESP's adsorption efficiency. FTIR analysis identified the functional groups of ESP, MESP, and MESPMC. XRD analysis reveals a hexagonal crystal structure of calcite in MESP and a combination of the hexagonal crystal structure of calcite and the cubic crystal structure of iron in MESPMC. The Scherrer equation is used to determine the average crystallite sizes of MESP and MESPMC, which are 22.59 nm and 12.15 nm, respectively. The SEM image shows the irregular shape of the MESP and MESPMC particles, as well as the active coating layer in MESPMC. EDX analysis reveals that Ca (20.92 %), O (56.83 %), and Fe (41.03 %), O (48.83 %) are the most abundant elements in MESP and MESPMC respectively. TGA analysis points out that MESPMC outperforms MESP in terms of thermal stability between 600 and 750 °C. MESP and MESPMC were found to be very efficient adsorbent for lead and methylene blue in aqueous medium. At 40 mg/mL adsorbent dosage, ESP, MESP, and MESPMC had the highest yields of Pb^{2+} removal, with 46.996 %, 99.27 %, and 99.78 % respectively at 200 rpm for 60 min with 25 °C. Furthermore, at the 0.5 mg/mL adsorbent dosage, ESP, MESP, and MESPMC have the maximum removal efficiency of methylene blue, with 47.19 %, 90.1 %, and 92 %, respectively at 200 rpm for 30 min with 25 °C. In both cases, the removal efficiency of MESPMC is slightly higher than that of MESP and much higher than that of ESP. Additionally, the results confirm that MESP and MESPMC are potential environment-friendly bio sources to remediate heavy metal (Pb^{2+}) and methylene blue dye from water.

* Corresponding author.
E-mail addresses: rabbi_chem@yahoo.com, ahasanurrabbi@bcsir.gov.bd (M.A. Rabbi).

https://doi.org/10.1016/j.heliyon.2024.e36160
Received 14 June 2024; Received in revised form 1 August 2024; Accepted 11 August 2024
Available online 13 August 2024

1. Introduction

The use of composite particles has grown over time in a variety of sectors, including drug delivery, imaging, semiconductor fabrication, catalysts, water purification, and air purification. Composites are intriguing materials for applications as catalysis, due to their high surface areas coupled with improved electronic/optical characteristics as compared with other pure materials [1]. Among these, water purification with composites is a popular, inexpensive, and effective technology. Most of the industries treat their industrial wastewater improperly and release it into the environment [2]. These impure waters may contain inorganic anionic contaminants such as chromate, F^{-}, arsenite and arsenate, etc. or inorganic cationic contaminants such as heavy metals: lead, mercury, cadmium, zinc, etc. [3]. Again, some industries like textile, dairy, biomedical, pharmaceuticals, distillery, and cannery discharge organic wastes such as synthetic drugs, dyes, and microbes [4].

Heavy metals are a substantial source of pollution in the environment. Heavy metals enter the environment as a result of increased agricultural and industrial activity. These elements have an atomic weight of 63.5 u - 200.6 u and a specific gravity greater than 5 [5]. The USEPA classified metals such as chromium, copper, zinc, cadmium, cobalt, lead, and nickel as hazardous [6]. Among these heavy metals, lead is one of the heavy metals that enter the environment via metal pigments, paints, gasoline, batteries, fabrication, and corrosion. It damages the nervous systems, kidney, brain, reproductive, liver, and accumulates in the tissues of both humans and animals. It has the potential to cause serious health issues such as stillbirths, infertility, abortion, and neonatal deaths. It impairs calcium metabolism and vitamin D, changes hemoglobin synthesis, and results in anemia [7].

According to past research, more than 80 % of industrial wastewater contains contaminants that are discharged into the environment without treatment [8]. Among these contaminants, synthetic dyes are the main wastewater pollutants [9]. Organic wastes, such as dyes, are usually hazardous to aquatic ecosystems and ruining the aesthetics of the water bodies [10]. Generally, the dyes' color reduces light absorption in the water, which lowers the photosynthetic rate and DO, and affects the whole aquatic biota. Dyes are also carcinogenic, poisonous, and mutagenic chemicals that can infiltrate the food chain and impair human health [11–13]. Water pollution can also occur spontaneously. For example, arsenic pollution is a major problem in Bangladesh, West Bengal (India), and Nepal as a result of the weathering of arsenic-containing rocks [14].

Heavy metals and dyes are removed by precipitation, oxidation/reduction, and membrane filtration methods such as reverse osmosis and ion exchange [15]. However, using these approaches, separating metal or dyes concentrations smaller than 100 mg/L becomes problematic [16]. Adsorption is a commonly used, cost-effective, and environmentally friendly alternative to these procedures. Adsorption is essentially a mass transfer process in which a substance is transported from the liquid phase to the surface of a solid and becomes attached by physical and/or chemical interactions [17]. It is capable of meeting water reuse requirements and industry's stringent effluent regulations. Adsorption may remove both soluble and insoluble chemicals, as well as biological pollutants, with an efficiency of 90–99 % [18].

Adsorbent selection is a very critical issue for the efficiency, operation and development of adsorption processes. An efficient adsorbent should have a strong adsorption interaction with the target contaminants in addition to a high removal capacity. These adsorbents can be synthetic or natural [19]. Activated carbons (ACs), graphene-based materials, clay minerals, zeolites, carbon nanotubes, polymeric materials, and biomass are some of the most frequent adsorbent sources [20,21]. With the advent of the use of waste materials as adsorbents, numerous viable bio-wastes obtained from humans, birds, and animals, such as horns, nails, feathers, and hairs, have been employed as possible adsorbents for the removal of inorganic and organic chemicals [22]. Natural sources, such as water hyacinth, are chemically treated and dried to remove contaminants from water, including Cd(II) and Pb(II) [23,24]. Modified water hyacinth/chitosan was discovered to remove 90.6 % of lead ions from water in 180 min [25]. The polyoxometalate/titania composite also demonstrated superior lead adsorption ability [26]. Chemically treated *Ziziphus spina-christi stones* effectively absorbed Pb(II), Zn(II), and Cd(II) from wastewater in both single and ternary metal systems [27]. Among various types of adsorbents eggshell-based bio adsorbent is gaining popularity due to its availability and high adsorption rate [28,29]. The eggshell's inner and exterior layers are made up of calcined shell and shell membrane layers [30]. Eggshell is a waste material that is produced in huge amounts from sources such as poultry, residences, restaurants, bakeries, and food processing facilities. Bakeries and the food industry produce the most eggshell, and disposing of it has always been a challenge for the government [22]. Among various types of discarded eggshells, chicken eggshell waste is more prevalent. Recently, these waste chicken eggshells have been employed as an adsorbent for purifying wastewater [31,32]. The adsorption characteristics of basic yellow 28 dye on calcined eggshells were examined using batch tests. The findings indicated a 28.87 mg/g maximum biosorption capability [33]. Multilayer adsorption was shown using the Freundlich model, and this finding was consistent with research conducted by other scientists on the elimination of reactive red 123 dye, methylene blue, and brilliant green dye [34]. Eggshells are now being physically modified using a crusher and utilized to adsorb hexavalent chromium and cadmium from wastewater [35]. Other research indicates that thermal treatment of eggshells at high temperatures following physical treatment improves fluoride adsorption performance [36]. Furthermore, chemical treatments, such as sol-gel treatment, are utilized in conjunction with physical and thermal treatments to increase eggshell powder's surface area and efficiency [37]. Activating chemicals, such as NaOH and H_3PO_4, are used with the eggshell to reduce the heating requirement in thermal treatment and increase the surface area [38]. However, separating these particles from water after heavy metal or dye adsorption is a challenging issue. Additionally, the rapid recombination of e^{-}/h^{+} pairs in eggshell-based nanoparticles also poses a substantial obstacle to their industrial application, similar to other single-component nanoparticles. Heterojunction assembly has been used in the doping and manufacturing of composite materials to overcome these constraints. Appropriate heterojunction can more effectively suppress e^{-}/h^{+} relocation via controlling the charge kinetics [39]. However, recent developments in magnetic coating technology have made it possible to solve this separation challenge. For example, zeolites have been coated with magnetic particles to aid in the separation process following the adsorption of dye, heavy metal, and pharmaceutical waste from water [40]. Furthermore,

numerous types of materials have been coated with magnetic particles, resulting in good separation [41]. Eggshells are also being modified with magnetic particles to aid in the separation of particles and adsorbing efficiency [38]. Additionally, it modifies the surface area and accelerates the adsorption process. However, one significant disadvantage of iron oxide particles is that they agglomerate as an adsorbent due to their high surface-to-volume ratio and low surface energy. As a result, ironoxide particles are more effective when used as a surface modification agent on other materials [42]. This research focused on eggshell powder chemi-thermal modification and then making a magnetic composite using $FeCl_3$ and $FeSO_4$. Waste derived modified eggshell powder (MESP) is low-cost adsorbent and eggshell/ironoxide powder magnetic composite (MESPMC) makes it easily separable form the water medium. The structural, morphological, and optical features of the produced MESP and MESPMC were determined using XRD, SEM, TGA and FT-IR spectroscopy. A UV–visible spectrophotometric approach was used to analyze the elimination of methylene blue using eggshell powder (ESP), modified eggshell powder (MESP) and modified eggshell/iron oxide powder magnetic composite (MESPMC) as adsorbent. The proportion of Pb^{2+}removal using ESP, MESP and MESPMC was measured using an Atomic Absorption Spectrophotometer (AAS).

2. Materials and methods

Chicken eggshells were collected from RUET Cafeteria, Rajshahi, Bangladesh. Orthophosphoric acid (H_3PO_4; Purity ≥85 % in H_2O), Iron (III) chloride hexahydrate ($FeCl_3.6H_2O$; Purity ≥97 %), Iron (II) sulfate heptahydrate ($FeSO_4.7H_2O$; Purity ≥99 %), Sodium Hydroxide (NaOH; Purity ≥98 %) were purchased from Sigma-Aldrich. Lead nitrate was acquired from Merck, Germany (Purity ≥99.5 %).

2.1. Eggshell powder (ESP) preparation

Chicken eggshells were gently cleaned with water and washed many times with double distilled water to remove contaminants. After reaching a steady weight, the eggshells were dried in an oven dryer for 24 h and then crushed using a mortar and grinder. After screening to a geometrical particle size of 75–180 μm with a metal sieve, ESP were stored in an airtight container at room temperature for later use.

2.2. Modified eggshell powder (MESP) preparation

For chemical activation, a glass beaker is placed on a magnetic stirrer and continuously stirred at 300 rpm 50 °C with 40 mL water and 10 g eggshell powder. Then, when the pH of the suspension is stable, 4 mL of H_3PO_4 is added at a rate of 1 mL/min as an activating agent. The sample is then constantly stirred for 2 h to allow the reaction of the activating agent and the sample to occur. The sample was then left to soak at room temperature for 72 h, then separated from the liquid using 0.50 μm syringe filter. And then the separated solid is repeatedly washed with distilled water and kept in a dryer at 110 °C for 1 day. Finally, the dry sample is taken to powder form by using mortar pestle. After that, this chemically activated fine powder is placed in a muffle furnace at 550 °C for 2 h for thermal activation. The powder is then grounded again using mortar and pestle. The crushed powder is then washed with 1 M HCl to remove any remaining organic material. Then it is cleaned numerous times with distilled water until the pH reaches 6–7. Then it is dried overnight at 110 °C.

2.3. Preparation of modified eggshell/ironoxide powder magnetic composite (MESPMC)

3.9 g of $FeCl_3.6H_2O$ and 1.9 g of $FeSO_4.7H_2O$ were mixed with 200 mL of water in a 500 mL conical flask, and then stirred at 300 rpm with a magnetic stirrer at 70 °C. Ironoxide nanoparticles (Fe_3O_4) contain both Fe^{2+} and Fe^{3+} in one compound. Hence two precursors, one containing divalent iron ($FeSO_4$) and one containing trivalent iron ($FeCl_3$) are used to prepare Fe_3O_4 nanoparticles. Ferric (Fe^{3+}) and ferrous (Fe^{2+}) in an aqueous mixture are mixed at a 2:1 M ratio [43]. Then 1 g of MESP was added on that suspension gradually. After that 1 M NaOH was added dropwise while stirring until the pH reached 10–11. It was then continuously agitated at 70 °C for 3 h. The sample was then kept at room temperature for 24 h. After that, the composite was easily separated with a magnet. Finally, the separated sample was rinsed repeatedly with distilled water to neutralize the pH and then dried overnight in a hot air oven at 110 °C. Finally, the dried MESPMC was grinded using mortar pestle.

2.4. Characterization of MESP and MESPMC

Several analyses were performed to assess the properties of the adsorbent, including FTIR, XRD, SEM, EDX and TGA.

A Fourier Transform Infrared (FTIR) spectrometer (PerkinElmer FTIR-1400, UK) was used for analyzing the structural properties of ESP, MESP, and MESPMC. Before investigation, the materials were vacuum dried at a low temperature of 50 °C and pressed into pellets. At room temperature, the samples were scanned using the deflection mode in the range of 4000 to 400 cm^{-1}.

X-ray diffraction (XRD) analysis of MESP and MESPMC were performed using LabX Shimadzu equipment that irradiated Cu-Ka rays at 40 kV throughout a 2-h range of 10–80° at a scanning rate of 2°/minute. Additionally, Scherrer's equation was used to calculate the average crystallite size[44,45].

$$D = \frac{0.90\,\lambda}{\beta \cos\theta} \times 100 \quad (1)$$

here,

D is the size of the crystallite,

λ is the X-ray wavelength used,

β is the entire line width at half-maximum height of the primary intensity peak,

θ is the Bragg angle,

and 0.90 is the Debye-Scherrer constant.

JSM-IT800is (JEOL, Japan) was used to take ultra-high resolution SEM pictures. The samples were gold coated using a smart coater (DII-29030-SCTR) before being imaged using a SEM. SEM image of MESP and MESPMC were obtained with a working voltage range of 5–25 kV. An EDX spectroscopy adapter that was built-in to the SEM was used to record the EDX spectra.

The thermal characteristics of 10.0 mg of dry MESP and MESPMC powder samples were determined using a thermogravimetric analyzer (TGA) (STA 8000, PerkinElmer, Netherlands). The samples were dried in a flowing nitrogen environment at a rate of 20 °C/min, and the percentage of mass loss was measured.

2.5. Experimental methodology for heavy metal removal

2.5.1. Adsorbate solution preparation

A metal stock solution containing Pb^{2+} ions was prepared by adding 640 mg of $Pb(NO_3)_2$ in 500 mL of deionized water. The stock solution was diluted to the desired concentrations with deionized water. NaOH and H_2SO_4 are used to neutralize this solution.

2.5.2. Experimental methodology for Pb^{2+} adsorption by using ESP, MESP and MESPMC

25 mL of adsorbate was collected in each conical flask with a lead content of 9.643 ppm. Each sample obtained 4 mg/mL, 10 mg/mL, 20 mg/L, 30 mg/L, 40 mg/L of ESP and then shaken in a rotary shaker at 200 rpm for 60 min with 25 °C. The treated solution is then centrifuged and then filtered with 0.50 μm syringe filter to separate it from the adsorbent, and then Analyst 400 PerkinElmer Atomic Absorption Spectrometer (AAS) Flame was used to analyze Pb^{2+} concentrations in samples using the standard calibration procedure. Utilizing a range of calibration standards (5–200 ppm), a sample solution was analyzed. The standard calibration curve was then used to calculate the amount of metal in each sample [46]. The removal efficiency of Pb^{2+} from the aqueous solution was calculated using the following equation:

$$\eta = \frac{(C0 - Ce)}{C0} \times 100 \quad (2)$$

here,

η is Pb^{2+} removal efficiency,

Co (mg/L) is the initial metal ion concentration,

Ce (mg/L) is the final metal ion concentration,

The Pb^{2+} removal efficiency was determined using the MESP and MESPMC adsorbent by following the same procedure.

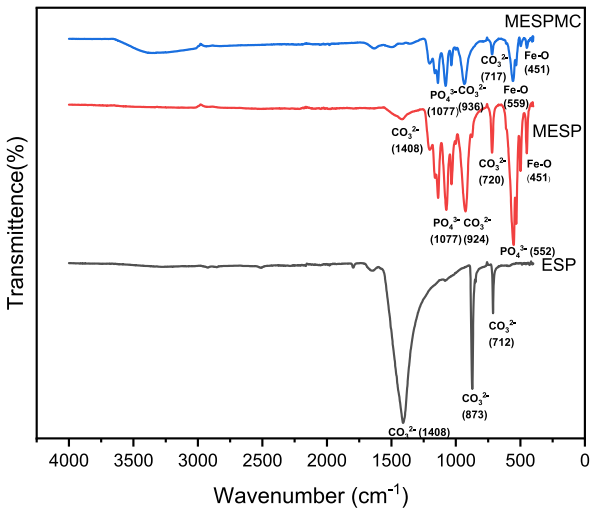

Fig. 1. FTIR spectra of ESP, MESP and MESPMC.

2.5.3. Experimental methodology for methylene blue removal by using ESP, MESP and MESPMC

20 mL of adsorbate was collected in each conical flask with a very trace amount of methylene blue in it. After that, each sample obtained 0.1 mg/mL, 0.2 mg/mL, 0.3 mg/mL, 0.4 mg/mL, and 0.5 mg/mL of ESP were shaken for 30 min at 200 rpm in a rotary shaker at 25 °C. The treated solution is then centrifuged and then filtered with 0.50 μm syringe filter to separate it from the adsorbent. A UV–Vis spectrophotometer (Germany; Spectrum 500 D) is used to assess the absorbance of this solution at 665 nm since MB showed absorption at that wavelength [38].

The removal efficiency of MB from the aqueous solution was calculated using the following equation:

$$\varepsilon = \frac{(A0 - Ae)}{A0} \times 100 \quad (3)$$

here, ε is dye (MB) removal efficiency,

Ao (a.u) is initial absorbance at 665 nm,

Ae (a.u) is final absorbance at 665 nm.

And by employing the same process with the MESP and MESPMC adsorbent, the concentration of treated solutions was ascertained.

3. Result and discussion

3.1. Fourier transform infrared spectroscopy

Fig. 1 depicts the FTIR spectra for ESP, MESP, and MESPMC. The peaks at 1408 cm^{-1} at ESP and MESP are due to carbonate group vibration. The phosphate group is represented by the bands found at MESP and MESPMC at 1077 cm^{-1}. Bands at 924 cm^{-1} and 936 cm^{-1} at MESP and MESPMC indicate the presence of calcium carbonate [38]. The band seen at 873 cm^{-1} at MESP corresponds to the vibration of Calcite [47]. Peaks at 712 cm^{-1}, 720 cm^{-1} and 717 cm^{-1} for ESP, MESP and MESPMC respectively, are due to the calcite out of plane bending [48]. Peaks at 552 cm^{-1} at MESP indicated the presence of phosphate ion vibrations [49]. Peaks at 559 cm^{-1} at MESPMC and 451 cm^{-1} at MESPMC and MESP indicate Fe–O stretching vibrations [50]. Carbonate group vibration at 1408 cm^{-1} was eliminated at MESPMC due to the modification. This modification increases the surface area of particles and, therefore, the adsorption rate.

3.2. X-Ray diffraction (XRD) analysis

The structure and crystalline phase of MESP and MESPMC were investigated using XRD peaks. The XRD patterns are shown in Fig. 2. MESP's XRD peaks at 26.8°, 29.42°, 30.58°, 36.02°, 39.44°, 43.18°, 47.54°, 48.54°, and 57.46° match to Braggs reflection planes at 112, 201, 202, 204, 205, 206, 207, 304, and 314, respectively. These peaks match JCPDS: 721616, confirming the presence of $CaCO_3$ in MESP and indicating its hexagonal crystal structure [51]. Furthermore, the peak at 23.1° corresponds to the (012) reflection plane, which represents the rhombohedral structure of $CaCO_3$ [38]. Again, XRD peaks observed for MESPMC at 18.36°, 35.66°, 40.72°, 43.42°, 57.38°, 62.8°, and 63.9° correspond to Braggs reflection planes of 111, 311, 321, 400, 511 and 440 respectively. These peaks are consistent with JCPDS: 040755, confirming the presence of maghemite (Fe_2O_3) in MESPMC and its cubic crystal shape [52]. Furthermore, the peaks detected at 26.8°, 29.42°, and 30.58° correspond to the 112, 201, and 202 reflection planes, showing the presence of hexagonal structured $CaCO_3$, which is consistent with MESP XRD peaks. These peaks suggest that $FeCl_3$ and $FeSO_4$ were properly coated over MESP and formed magnetic composites, however, the peak intensity was somewhat changed, probably due to the interaction between the crystalline phases of $CaCO_3$ and Fe_2O_3. Moreover, the average crystallite size for MESP is 22.59 nm, but the

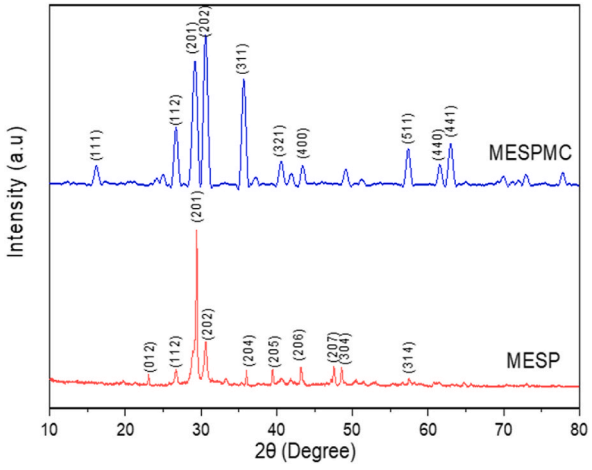

Fig. 2. XRD graph of MESP and MESPMC.

average crystallite size for MESPMC is 12.15 nm, according to Scherrer's eq. (1) [44,45]. In this case, the iron coating in MESPMC forms a composite, which may increase the active site on the sorbent and thereby cause the crystallite size to decrease.

3.3. Scanning electron microscopy (SEM) and energy dispersive X-ray spectroscopy (EDX)

The surface morphology and qualitative elemental analysis of MESP and MESPMC were determined using a scanning electron microscope (SEM) with energy-dispersive X-ray spectroscopy (EDX). Fig. 3(a, c) shows the SEM images of MESP and MESPMC. These images demonstrate that the MESP and MESPMC particles have a non-uniform shape. Fig. 3(c) also shows a layer of tiny particles on the MESP particles, which normally indicates the presence of Fe_2O_3 particles, implying that the particles are agglomerated and adhered to one another, resulting in the formation of MESPMC. Fig. 3(b, d) show the elemental compositions of MESP and MESPMC, respectively. The most prevalent components in MESP were calcium (20.92 %) and oxygen (56.83 %), followed by phosphorus (17.44 %) and carbon (4.82 %). Whereas MESPMC's most abundant components were Fe (41.03 %), O (48.83 %), alongside with Ca (8.34 %), and C (1.79 %).

3.4. Thermogravimetric analysis (TGA)

The thermal behavior of MESP and MESPMC was examined using Thermogravimetric Analysis (TGA), and the findings are presented in Fig. 4. The results show that MESP and MESPMC weight reduction can be separated into three stages. The first stage weight loss was found between 50 and 120 °C, with MESP and MESPMC losing 11.34 % and 22.214 %, respectively. This sort of weight loss occurs owing to the evaporation of moisture contained throughout the particles. At 130–380 °C, MESPMC lost 9.789 % of its weight, which was attributed to $FeCl_3$ degradation [53]. At 600–750 °C, MESP experiences a greater weight loss (13.68 %) due to $CaCO_3$ decomposition into CaO and CO_2 [54]. Decomposition in MESPMC begins at 380 °C due to the decomposition of $FeSO_4$ [55]. However, the weight loss rate of MESPMC at 380–800 °C is lower than that of MESP because the coated Fe particles in MESPMC prevent it from decomposing.

3.5. Comparative performance on Pb^{2+} removal of various adsorbents (ESP, MESP and MESPMC)

The adsorption activity of Pb^{2+} in ESP, MESP, and MESPMC were measured using Atomic Adsorption Spectrophotometric method. The amount of adsorbent in 20 mL adsorbate is increased from 4 mg/mL to 40 mg/mL. Additionally, Pb^{2+} removal efficiency is

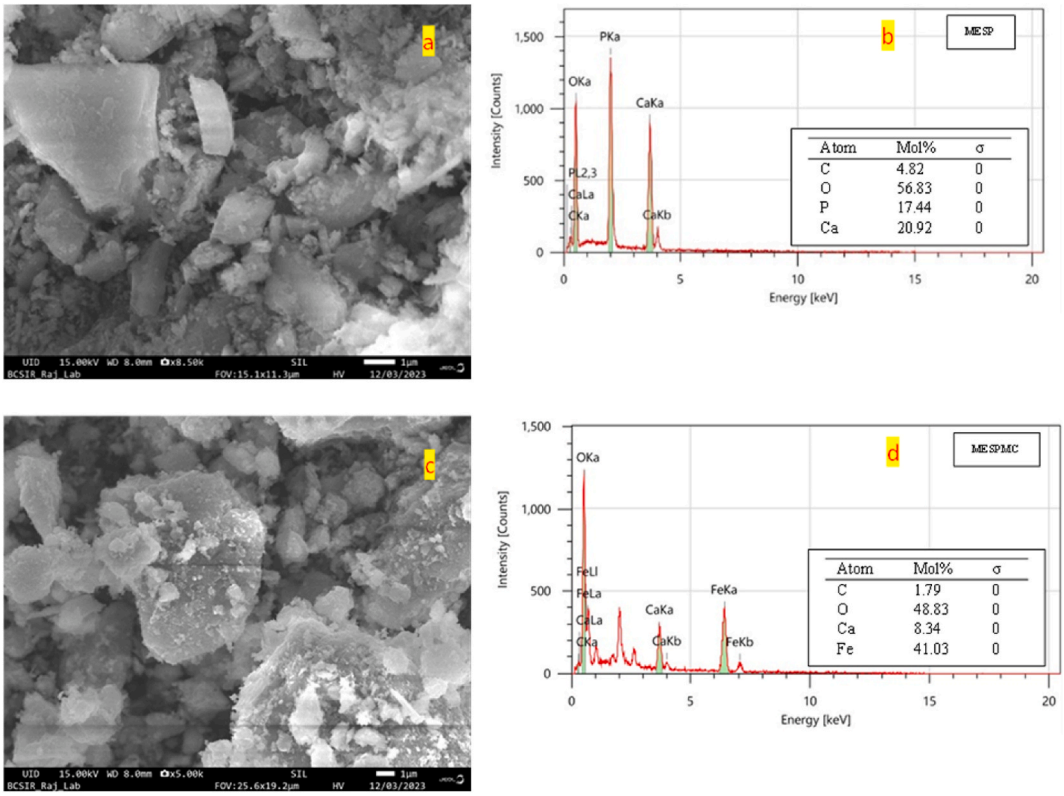

Fig. 3. a) SEM image of MESP; b) EDX spectra of MESP; c) SEM image of MESPMC; d) EDX spectra of MESPMC.

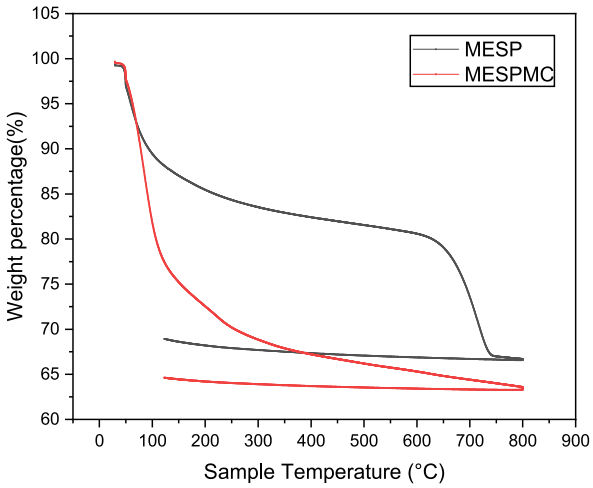

Fig. 4. TGA analysis graph of MESP & MESPMC.

calculated using equation (2). Table 1 shows that the final concentration of Pb^{2+} using ESP, MESP, and MESPMC decreases as the adsorbent dosage increases. Moreover Fig. 5 shows that the adsorption efficiency of ESP range from 22.01 % to 46.996 % as the adsorbent dose was raised from 4 mg/mL to 40 mg/mL. Similarly, the adsorption efficiency of MESP and MESPMC range from 89.74 % to 99.27 % and 91.38 %–99.78 %, respectively, as the adsorbent dose was increased from 4 mg/mL to 40 mg/mL. In every case, the rate of Pb^{2+} uptake increases with increasing adsorbent dose. This is because there is a significant increase in both the composite surface area and the total amount of active adsorption site when the adsorbent dosage increases. As a result, a higher removal percentage is achieved by adsorbing more Pb^{2+} from the solution [56].

For 30 mg/mL and 40 mg/mL adsorbent, the Pb^{2+} removal efficiency of MESP is 99.12 %, 99.27 %, and MESPMC is 99.77 %, 99.78 %. The Pb^{2+} removal efficiency difference is quite low here. This may be due to the fact that the sorbent's surface has been saturated and is on the verge of reaching equilibrium. The Lagergren (Pseudo first order) model states that the adsorption rate is determined by the accessible sites in the adsorbent for the physisorption process [57].

Again, MESP and MESPMC have higher Pb^{2+} removal efficiency than ESP. This is because the thermal treatments have enhanced the active adsorption site in MESP and MESPMC [58]. Additionally, the Pb^{2+}removal efficiency of MESPMC is slightly greater than that of MESP for all adsorbent doses as the iron coating in MESPMC form composite thus increasing the active site on sorbent [56].

3.6. Comparative performance on methylene blue removal of various adsorbents (ESP, MESP and MESPMC)

The efficiency of removing methylene blue (MB) is correlated with the dye-adsorbing activity of ESP, MESP, and MESPMC. The UV–visible irradiation method was used to measure the MB adsorbing activity of ESP, MESP and MESPMC. Additionally, equation (3) is used to calculate the MB removal efficiency of ESP, MESP, and MESPMC, which is represented in Fig. 6.

Initially, the absorbance for a trace amount of MB in water was 1.2565 a. u. at 665 nm. Table 2 points out that as the ESP, MESP, and MESPMC adsorbent dose rises, the absorbance at 665 nm decreases. Furthermore, Fig. 6 indicates that increasing the ESP, MESP, and MESPMC dosage from 0.1 mg/mL to 0.5 mg/mL increases efficiency from 25.5 % to 47.19 %, 60 %–90.1 %, and 65 %–92 % for ESP, MESP, and MESPMC respectively. Here, the increase in adsorbent dosages may be attributed to an increase in the surface area and the availability of more active sites of adsorbents, which increase the MB removal efficiency [59]. Dye is adsorbed on ESP, MESP, and MESPMC through a mechanism with four different steps, including dye diffusion from the bulk of the solution to the adsorbent, pore diffusion, monolayer adsorption of dye molecules, and multilayer adsorption of dye molecules [60]. Heavy metals, such as Pb^{2+}, are similarly adsorbed. Organic contaminants, including dye, are removed through π-π interactions, H-bonding, electrostatic, and hydrophobic interactions [61]. On the other hand, most inorganic compound adsorption occurs as a result of electrostatic interactions

Table 1
Effect of adsorbent dose on Pb^{2+} Removal.

Adsorbent Dose (mg/mL)	Initial concentration of Pb^{2+} (mg/L)	ESP	MESP	MESPMC
		Final concentration of Pb^{2+} (mg/L)	Final concentration of Pb^{2+} (mg/L)	Final concentration of Pb^{2+} (mg/L)
4	9.6463	7.5225	0.8925	0.8310
10	9.6463	6.9232	0.1287	0.0991
20	9.6463	6.2225	0.0578	0.0237
30	9.6463	5.6223	0.0524	0.0219
40	9.6463	5.1129	0.0513	0.0208

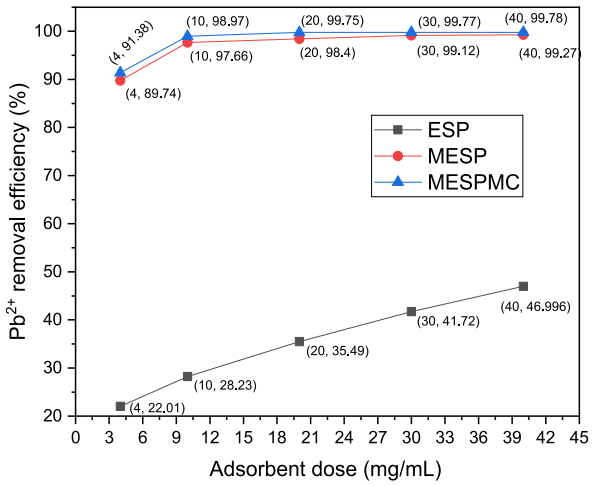

Fig. 5. Pb^{2+} removal efficiency of ESP, MESP and MESPMC.

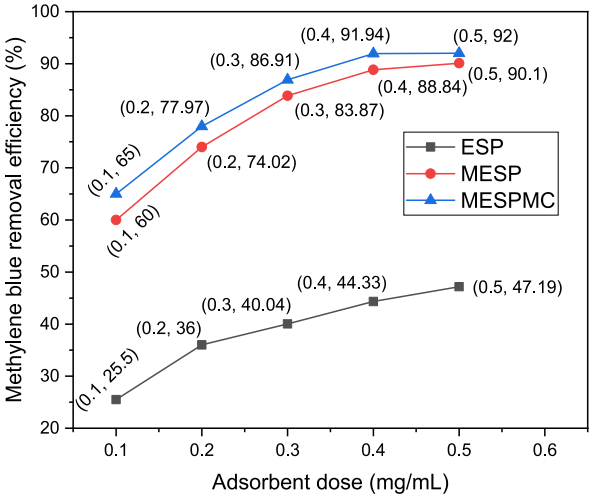

Fig. 6. Methylene blue removal efficiency of ESP, MESP and MESPMC.

Table 2
Effect of adsorbent dose on dye (methylene blue) removal.

Adsorbent Dose (mg/mL)	Initial absorbance of methylene blue (a.u)	ESP	MESP	MESPMC
		Final absorbance (a.u)	Final absorbance (a.u)	Final absorbance (a.u)
0.1	1.2565	0.9361	0.5026	0.4398
0.2	1.2565	0.8041	0.3264	0.2768
0.3	1.2565	0.7534	0.2026	0.1645
0.4	1.2565	0.6534	0.1042	0.1013
0.5	1.2565	0.5620	0.1260	0.1005

[62].

For 0.4 g and 0.5 g adsorbents, MESP has an MB removal efficiency of 88.84 %, 90.1 %, and MESPMC has an efficiency of 91.94 % and 92 % respectively. The rate of efficiency increase is minimal in this case, implying that adsorption capacity is decreasing. The reason for this is that the sorbent's surface may become saturated with MB and is close to equilibrium [63].

Again, MB removal efficiency is higher for MESP and MESPMC than for ESP. This might be a result of MESP and MESPMC's thermal treatment, which raises the active site and hence the efficiency [64]. Furthermore, the MB removal efficiency of MESPMC is somewhat larger than that of MESP for all adsorbent doses because the iron coating in MESPMC forms a composite, increasing the active site on the sorbent [65].

4. Conclusion

The present research successfully converted eggshell powder (ESP) into modified eggshell powder (MESP) and then into modified eggshell powder magnetic composite (MESPMC). The functional groups present in ESP, MESP, and MESPMC are revealed by FTIR analysis. The MESP XRD pattern indicates a mixed phase of calcite with a hexagonal crystal structure. Additionally, Scherrer equation indicates the average crystallite sizes of 22.59 nm and 12.15 nm for MESP and MESPMC respectively. On the other hand, MESPMC's XRD pattern revealed a combination of calcite's hexagonal crystal structure and iron's cubic structure. The SEM images identified an irregular shape of MESP and MESPMC particles with micro-pores, as well as an iron coating layer in MESPMC. EDX analysis confirmed the presence of Ca, O, C, and P in MESP, as well as Ca, Fe, O, and C in MESPMC. TGA analysis shows that MESPMC had lesser weight loss than MESP. The maximum MB removal efficiency of 47.19 %, 90.1 %, and 92 % were achieved at 0.5 mg/L ESP, MESP, and MESPMC doses, respectively with 200 rpm for 30 min and 25 °C, while the highest Pb^{2+} removal efficiency of 46.996 %, 99.27 %, and 99.78 % were obtained at 40 mg/L ESP, MESP, and MESPMC doses, respectively with 200 rpm for 60 min and 25 °C. Based on these findings, we can conclude that MESP and MESPMC are excellent adsorbents for Pb^{2+} and methylene blue removal from water.

CRediT authorship contribution statement

Maherab Hossain: Writing – original draft, Methodology, Investigation, Formal analysis. **Raihan Islam:** Visualization, Investigation. **Mohammad Nurur Rahman:** Supervision, Project administration. **Md Ibna Sabit Khan:** Validation, Investigation, Formal analysis. **Firoz Ahmed:** Validation, Data curation. **Md. Al-Amin:** Validation, Data curation. **M. Ahasanur Rabbi:** Writing – review & editing, Supervision, Methodology, Conceptualization.

Declaration of competing interest

The authors confirm that they have no conflicts of interest.

Acknowledgment

This work was supported by the Bangladesh Council of Scientific and Industrial Research.

References

[1] S.M. Reduwan Billah, Composites and Nanocomposites, 2019, pp. 1–67, https://doi.org/10.1007/978-3-319-92067-2_15-1.
[2] J. Ahmed, A. Thakur, A. Goyal, Industrial wastewater and its toxic effects, in: Biological Treatment of Industrial Wastewater, The Royal Society of Chemistry, 2021, pp. 1–14, https://doi.org/10.1039/9781839165399-00001.
[3] A. Ghosh, A.K. Nayak, A. Pal, Nano-particle-mediated wastewater treatment: a review, Curr Pollut Rep 3 (1) (Mar. 2017) 17–30, https://doi.org/10.1007/s40726-016-0045-1.
[4] H. Ben Slama, et al., Diversity of synthetic dyes from textile industries, discharge impacts and treatment methods, Appl. Sci. 11 (14) (Jul. 2021) 6255, https://doi.org/10.3390/app11146255.
[5] R. Foroutan, et al., Nickel ions abatement from aqueous solutions and shipbuilding industry wastewater using ZIF-8-chicken beak hydroxyapatite, J. Mol. Liq. 356 (Jun. 2022) 119003, https://doi.org/10.1016/j.molliq.2022.119003.
[6] M.H. Moslehi, M. Eslami, M. Ghadirian, K. Nateq, B. Ramavandi, N. Nasseh, Photocatalytic decomposition of metronidazole by zinc hexaferrite coated with bismuth oxyiodide magnetic nanocomposite: advanced modelling and optimization with artificial neural network, Chemosphere 356 (May 2024) 141770, https://doi.org/10.1016/j.chemosphere.2024.141770.
[7] O.I. Ali, E.R. Zaki, M.S. Abdalla, S.M. Ahmed, Mesoporous Ag-functionalized magnetic activated carbon-based agro-waste for efficient removal of Pb(II), Cd(II), and microorganisms from wastewater, Environ. Sci. Pollut. Control Ser. 30 (18) (Mar. 2023) 53548–53565, https://doi.org/10.1007/s11356-023-26000-w.
[8] S.H. Teo, et al., Sustainable toxic dyes removal with advanced materials for clean water production: a comprehensive review, J. Clean. Prod. 332 (Jan. 2022) 130039, https://doi.org/10.1016/j.jclepro.2021.130039.
[9] S.J. Peighambardoust, D.C. Boffito, R. Foroutan, B. Ramavandi, Sono-photocatalytic activity of sea sediment@400/ZnO catalyst to remove cationic dyes from wastewater, J. Mol. Liq. 367 (Dec. 2022) 120478, https://doi.org/10.1016/j.molliq.2022.120478.
[10] A.K.D. Alsukaibi, Various approaches for the detoxification of toxic dyes in wastewater, Processes 10 (10) (Sep. 2022) 1968, https://doi.org/10.3390/pr10101968.
[11] B. Lellis, C.Z. Fávaro-Polonio, J.A. Pamphile, J.C. Polonio, Effects of textile dyes on health and the environment and bioremediation potential of living organisms, Biotechnology Research and Innovation 3 (2) (Jul. 2019) 275–290, https://doi.org/10.1016/j.biori.2019.09.001.
[12] M.M. Hassan, C.M. Carr, A critical review on recent advancements of the removal of reactive dyes from dyehouse effluent by ion-exchange adsorbents, Chemosphere 209 (Oct. 2018) 201–219, https://doi.org/10.1016/j.chemosphere.2018.06.043.
[13] M. Imran, D.E. Crowley, A. Khalid, S. Hussain, M.W. Mumtaz, M. Arshad, Microbial biotechnology for decolorization of textile wastewaters, Rev. Environ. Sci. Biotechnol. 14 (1) (Mar. 2015) 73–92, https://doi.org/10.1007/s11157-014-9344-4.
[14] S.J. Tesh, T.B. Scott, Nano-composites for water remediation: a review, Adv. Mater. 26 (35) (Sep. 2014) 6056–6068, https://doi.org/10.1002/adma.201401376.
[15] N.A.A. Qasem, R.H. Mohammed, D.U. Lawal, Removal of heavy metal ions from wastewater: a comprehensive and critical review, NPJ Clean Water 4 (1) (Jul. 2021) 36, https://doi.org/10.1038/s41545-021-00127-0.
[16] A. Abdolali, W.S. Guo, H.H. Ngo, S.S. Chen, N.C. Nguyen, K.L. Tung, Typical lignocellulosic wastes and by-products for biosorption process in water and wastewater treatment: a critical review, Bioresour. Technol. 160 (May 2014) 57–66, https://doi.org/10.1016/j.biortech.2013.12.037.
[17] S. Dutta, R.K. Sharma, Sustainable Magnetically Retrievable Nanoadsorbents for Selective Removal of Heavy Metal Ions from Different Charged Wastewaters, 2019, pp. 371–416, https://doi.org/10.1016/B978-0-12-815730-5.00015-6.
[18] N. Kasera, P. Kolar, S.G. Hall, Nitrogen-doped biochars as adsorbents for mitigation of heavy metals and organics from water: a review, Biochar 4 (1) (Dec. 2022) 17, https://doi.org/10.1007/s42773-022-00145-2.
[19] P. Pourhakkak, M. Taghizadeh, A. Taghizadeh, M. Ghaedi, Adsorbent, 2021, pp. 71–210, https://doi.org/10.1016/B978-0-12-818805-7.00009-6.
[20] N.H. Solangi, J. Kumar, S.A. Mazari, S. Ahmed, N. Fatima, N.M. Mubarak, Development of fruit waste derived bio-adsorbents for wastewater treatment: a review, J. Hazard Mater. 416 (Aug. 2021) 125848, https://doi.org/10.1016/j.jhazmat.2021.125848.

[21] M. Boehler, B. Zwickenpflug, J. Hollender, T. Ternes, A. Joss, H. Siegrist, Removal of micropollutants in municipal wastewater treatment plants by powder-activated carbon, Water Sci. Technol. 66 (10) (Nov. 2012) 2115–2121, https://doi.org/10.2166/wst.2012.353.

[22] A. Mittal, M. Teotia, R.K. Soni, J. Mittal, Applications of egg shell and egg shell membrane as adsorbents: a review, J. Mol. Liq. 223 (Nov. 2016) 376–387, https://doi.org/10.1016/j.molliq.2016.08.065.

[23] M. Ibrahim, A.A. Shaltout, D.E. Atta, A.F. Jalbout, M. Soylak, Removal of COOH, Cd and Pb using water hyacinth: FTIR and flame atomic absorption study, J. Iran. Chem. Soc. 6 (2) (Jun. 2009) 364–372, https://doi.org/10.1007/BF03245846.

[24] H.S. Ibrahim, N.S. Ammar, M. Soylak, M. Ibrahim, Removal of Cd(II) and Pb(II) from aqueous solution using dried water hyacinth as a biosorbent, Spectrochim. Acta Mol. Biomol. Spectrosc. 96 (Oct. 2012) 413–420, https://doi.org/10.1016/j.saa.2012.05.039.

[25] N.S. Ammar, W. El hotaby, H.S. Ibrahim, S.A. El-Khodary, H. Elhaes, M.A. Ibrahim, Cost effective natural microspheres for the removal of Pb from wastewater, Curr Metabolomics 6 (1) (Jan. 2018), https://doi.org/10.2174/2213235X04666160926122105.

[26] E.A.-R. Assirey, M.E.M. Ali, N.S. Ammar, H.S. Ibrahim, M. Ibrahim, Novel composite for lead ions removal from wastewater, J. Comput. Theor. Nanosci. 14 (12) (Dec. 2017) 5735–5742, https://doi.org/10.1166/jctn.2017.7000.

[27] E.A. Assirey, S.M. Sirry, H.A. Burkani, M.A. Ibrahim, Modified Ziziphus spina-christi stones as green route for the removal of heavy metals, Sci. Rep. 10 (1) (Nov. 2020) 20557, https://doi.org/10.1038/s41598-020-76810-y.

[28] R. de O. Zonato, B.R. Estevam, I.D. Perez, V. Aparecida dos Santos Ribeiro, R.F. Boina, Eggshell as an adsorbent for removing dyes and metallic ions in aqueous solutions, Cleaner Chemical Engineering 2 (Jun. 2022) 100023, https://doi.org/10.1016/j.clce.2022.100023.

[29] A. Murcia-Salvador, J.A. Pellicer, M.I. Rodríguez-López, V.M. Gómez-López, E. Núñez-Delicado, J.A. Gabaldón, Egg by-products as a tool to remove direct blue 78 dye from wastewater: kinetic, equilibrium modeling, thermodynamics and desorption properties, Materials 13 (6) (Mar. 2020), https://doi.org/10.3390/ma13061262.

[30] S. Owuamanam, D. Cree, Progress of bio-calcium carbonate waste eggshell and seashell fillers in polymer composites: a review, Journal of Composites Science 4 (2) (Jun. 2020) 70, https://doi.org/10.3390/jcs4020070.

[31] J.M. Vonnie, K. Rovina, N.M.N. Aqilah, X.W.L. Felicia, Development and characterization of biosorbent film from eggshell/orange waste enriched with banana starch, Polymers 15 (11) (May 2023), https://doi.org/10.3390/polym15112414.

[32] A. Mittal, M. Teotia, R.K. Soni, J. Mittal, Applications of egg shell and egg shell membrane as adsorbents: a review, J. Mol. Liq. 223 (Nov. 2016) 376–387, https://doi.org/10.1016/j.molliq.2016.08.065.

[33] R. Slimani, et al., Calcined eggshells as a new biosorbent to remove basic dye from aqueous solutions: thermodynamics, kinetics, isotherms and error analysis, J. Taiwan Inst. Chem. Eng. 45 (4) (Jul. 2014) 1578–1587, https://doi.org/10.1016/J.JTICE.2013.10.009.

[34] M.A. Abdel-Khalek, M.K. Abdel Rahman, A.A. Francis, Exploring the adsorption behavior of cationic and anionic dyes on industrial waste shells of egg, J. Environ. Chem. Eng. 5 (1) (Feb. 2017) 319–327, https://doi.org/10.1016/J.JECE.2016.11.043.

[35] O.G. Abatan, P.A. Alaba, B.A. Oni, K. Akpojevwe, V. Efeovbokhan, F. Abnisa, Performance of eggshells powder as an adsorbent for adsorption of hexavalent chromium and cadmium from wastewater, SN Appl. Sci. 2 (12) (Dec. 2020) 1996, https://doi.org/10.1007/s42452-020-03866-w.

[36] J.-I. Lee, S.-H. Hong, C.-G. Lee, S.-J. Park, Fluoride removal by thermally treated egg shells with high adsorption capacity, low cost, and easy acquisition, Environ. Sci. Pollut. Control Ser. 28 (27) (Jul. 2021) 35887–35901, https://doi.org/10.1007/s11356-021-13284-z.

[37] C. Quan, M. Cortazar, L. Santamaria, G. Lopez, C. Wu, N. Gao, Valorization of waste eggshell for CO2 sorbents production by sol-gel citric acid treatment in a fixed-bed reactor, J. CO2 Util. 75 (Sep. 2023) 102562, https://doi.org/10.1016/j.jcou.2023.102562.

[38] A. Ahmad, et al., A novel study on synthesis of egg shell based activated carbon for degradation of methylene blue via photocatalysis, Arab. J. Chem. 13 (12) (Dec. 2020) 8717–8722, https://doi.org/10.1016/j.arabjc.2020.10.002.

[39] Y. Xie, M. Abaee, R. Navazeni, V. Shamshiri, Z. Frontistis, M. Amarzadeh, Engineering S-scheme heterojunction MgO/WO3-integrated Graphene photocatalyst for robust detoxification of tetracycline: mechanistic insight and actual matrix remediation, Surface. Interfac. 51 (Aug. 2024) 104591, https://doi.org/10.1016/j.surfin.2024.104591.

[40] M. Maharana, S. Sen, Magnetic zeolite: a green reusable adsorbent in wastewater treatment, Mater. Today Proc. 47 (2021) 1490–1495, https://doi.org/10.1016/j.matpr.2021.04.370.

[41] V. Phouthavong, et al., Magnetic adsorbents for wastewater treatment: advancements in their synthesis methods, Materials 15 (3) (Jan. 2022), https://doi.org/10.3390/ma15031053.

[42] M. Jain, M. Yadav, T. Kohout, M. Lahtinen, V.K. Garg, M. Sillanpää, Development of iron oxide/activated carbon nanoparticle composite for the removal of Cr (VI), Cu(II) and Cd(II) ions from aqueous solution, Water Resour. Ind. 20 (Dec. 2018) 54–74, https://doi.org/10.1016/J.WRI.2018.10.001.

[43] M.A. Rabbi, et al., Preparation of stable Fe_2O_3/Ag nanocomposite particles with catalytic, antioxidant and antibacterial properties, New J. Chem. 48 (12) (2024) 5278–5288, https://doi.org/10.1039/D3NJ05885A.

[44] M. Azqandi, et al., Intensified photo-decontamination of tetracycline antibiotic by S-scheme spinel manganese ferrite-grafted ZIF-8 heterojunction photocatalyst: mechanism conception, degradation pathway and DFT studies, J. Environ. Chem. Eng. 12 (3) (Jun. 2024) 112875, https://doi.org/10.1016/j.jece.2024.112875.

[45] M.H. Moslehi, M. Eslami, M. Ghadirian, K. Nateq, B. Ramavandi, N. Nasseh, Photocatalytic decomposition of metronidazole by zinc hexaferrite coated with bismuth oxyiodide magnetic nanocomposite: advanced modelling and optimization with artificial neural network, Chemosphere 356 (May 2024) 141770, https://doi.org/10.1016/j.chemosphere.2024.141770.

[46] M. Jaishankar, T. Tseten, N. Anbalagan, B.B. Mathew, K.N. Beeregowda, Toxicity, mechanism and health effects of some heavy metals, Interdiscipl. Toxicol. 7 (2) (Jun. 2014) 60, https://doi.org/10.2478/INTOX-2014-0009.

[47] S. Veerasingam, R. Venkatachalapathy, Estimation of carbonate concentration and characterization of marine sediments by Fourier Transform Infrared Spectroscopy, Infrared Phys. Technol. 66 (Sep. 2014) 136–140, https://doi.org/10.1016/j.infrared.2014.06.005.

[48] M.M.H. Al Omari, I.S. Rashid, N.A. Qinna, A.M. Jaber, A.A. Badwan, Calcium Carbonate, 2016, pp. 31–132, https://doi.org/10.1016/bs.podrm.2015.11.003.

[49] O.I. Ali, E.R. Zaki, M.S. Abdalla, S.M. Ahmed, Mesoporous Ag-functionalized magnetic activated carbon-based agro-waste for efficient removal of Pb(II), Cd(II), and microorganisms from wastewater, Environ. Sci. Pollut. Control Ser. 30 (18) (Mar. 2023) 53548–53565, https://doi.org/10.1007/s11356-023-26000-w.

[50] S. Fekri Aval, A. Akbarzadeh, M.R. Yamchi, F. Zarghami, K. Nejati-Koshki, N. Zarghami, Gene silencing effect of SiRNA-magnetic modified with biodegradable copolymer nanoparticles on hTERT gene expression in lung cancer cell line, Artif. Cells, Nanomed. Biotechnol. 44 (1) (Jan. 2016) 188–193, https://doi.org/10.3109/21691401.2014.934456.

[51] A. Amarasinghe, D. Wanniarachchi, Eco-Friendly photocatalyst derived from egg shell waste for dye degradation, J. Chem. 2019 (2019), https://doi.org/10.1155/2019/8184732.

[52] R. Nasiri, et al., Targeted delivery of bromelain using dual mode nanoparticles: synthesis, physicochemical characterization, in vitro and in vivo evaluation, RSC Adv. 7 (64) (Aug. 2017) 40074–40094, https://doi.org/10.1039/C7RA06389J.

[53] P. Agarwal, J.B. Preethi, D.K. Bora, Direct thermal decomposition of FeCl3.6H2O in oleic acid forms hematite cube and nano octahedron structure with quasicrystalline and supercell symmetries for enhanced photoelectrochemical functionality, Mater. Chem. Phys. 273 (Nov. 2021) 124977, https://doi.org/10.1016/j.matchemphys.2021.124977.

[54] P.R. Pandit, M.H. Fulekar, Egg shell waste as heterogeneous nanocatalyst for biodiesel production: optimized by response surface methodology, J. Environ. Manag. 198 (Aug. 2017) 319–329, https://doi.org/10.1016/J.JENVMAN.2017.04.100.

[55] A.H. Kamel, A.M. Abdallah, The thermal decomposition of ferrous sulphate heptahydrate. II. Decomposition to ferric oxide, Journal of Applied Chemistry and Biotechnology 22 (5) (May 1972) 599–602, https://doi.org/10.1002/jctb.2720220506.

[56] H. Li, T. Li, T. Zhang, J. Zhu, W. Deng, D. He, Construction and adsorption performance study of GO-CNT/activated carbon composites for high efficient adsorption of pollutants in wastewater, Polymers 14 (22) (Nov. 2022), https://doi.org/10.3390/POLYM14224951.

[57] B.M. Mercado-Borrayo, R. Schouwenaars, M.I. Litter, C.V. Montoya-Bautista, R.M. Ramírez-Zamora, Metallurgical slag as an efficient and economical adsorbent of arsenic, Water Reclamation and Sustainability (Jan. 2014) 95–114, https://doi.org/10.1016/B978-0-12-411645-0.00005-5.

[58] J.I. Lee, S.H. Hong, C.G. Lee, S.J. Park, Fluoride removal by thermally treated egg shells with high adsorption capacity, low cost, and easy acquisition, Environ. Sci. Pollut. Control Ser. 28 (27) (Jul. 2021) 35887–35901, https://doi.org/10.1007/S11356-021-13284-Z/METRICS.
[59] T. Liu, et al., Adsorption of methylene blue from aqueous solution by graphene, Colloids Surf. B Biointerfaces 90 (1) (Feb. 2012) 197–203, https://doi.org/10.1016/J.COLSURFB.2011.10.019.
[60] N.B. Singh, G. Nagpal, S. Agrawal, Rachna, Water purification by using adsorbents: a review, Environ. Technol. Innov. 11 (Aug. 2018) 187–240, https://doi.org/10.1016/j.eti.2018.05.006.
[61] V.I. Isaeva, et al., Modern carbon–based materials for adsorptive removal of organic and inorganic pollutants from water and wastewater, Molecules 26 (21) (Nov. 2021) 6628, https://doi.org/10.3390/molecules26216628.
[62] J.L. Figueiredo, M.F.R. Pereira, Porous texture versus surface chemistry in applications of adsorption by carbons, in: Novel Carbon Adsorbents, Elsevier, 2012, pp. 471–498, https://doi.org/10.1016/B978-0-08-097744-7.00015-6.
[63] Principles underlying the dyeing process, Modelling, Simulation and Control of the Dyeing Process, Jan. 2014, pp. 31–53, https://doi.org/10.1533/9780857097583.31.
[64] S.I. Eze, H.O. Abugu, O.A. Odewole, N.N. Ukwueze, L.O. Alum, Thermal and chemical pretreatment of Terminalia mantaly seed husk biosorbent to enhance the adsorption capacity for Pb2+, Sci Afr 15 (Mar. 2022) e01123 https://doi.org/10.1016/J.SCIAF.2022.E01123.
[65] A.G. El-Shamy, An efficient removal of methylene blue dye by adsorption onto carbon dot @ zinc peroxide embedded poly vinyl alcohol (PVA/CZnO2) nanocomposite: a novel Reusable adsorbent, Polymer 202 (Aug. 2020) 122565, https://doi.org/10.1016/J.POLYMER.2020.122565.